Article

Evaluation of Energy Absorption Capabilities of Polyethylene Foam under Impact Deformation

Baohui Yang [1,2], **Yangjie Zuo** [1,*] **and Zhengping Chang** [2]

1   School of Aeronautics and Astronautics, Sichuan University, 24 Nanyi Section Yihuan Road, Chengdu 610065, China; baohuiyang521@gmail.com
2   Department of Mechanical Engineering, Northwestern Polytechnical University, 127 Youyi Ave. West, Xi'an 710072, China; chzhping@nwpu.edu.cn
*   Correspondence: zuoyangjie@scu.edu.cn

Abstract: Foams are widely used in protective applications requiring high energy absorption under impact, and evaluating impact properties of foams is vital. Therefore, a novel test method based on a shock tube was developed to investigate the impact properties of closed-cell polyethylene (PE) foams at strain rates over 6000 s^{-1}, and the test theory is presented. Based on the test method, the failure progress and final failure modes of PE foams are discussed. Moreover, energy absorption capabilities of PE foams were assessed under both quasi-static and high strain rate loading conditions. The results showed that the foam exhibited a nonuniform deformation along the specimen length under high strain rates. The energy absorption rate of PE foam increased with the increasing of strain rates. The specimen energy absorption varied linearly in the early stage and then increased rapidly, corresponding to a uniform compression process. However, in the shock wave deformation process, the energy absorption capacity of the foam maintained a good stability and exhibited the best energy absorption state when the speed was higher than 26 m/s. This stable energy absorption state disappeared until the speed was lower than 1.3 m/s. The loading speed exhibited an obvious influence on energy density.

Keywords: foam; high strain rate; energy absorption; failure

1. Introduction

Polymeric foams are widely used in protective applications due to their high energy absorption capability [1–3], and the properties of a variety of open-cell and closed-cell foams have been widely studied under quasi-static compression [4–6], impact, and high strain rate loading conditions [7,8]. Foam materials and other materials can be combined into composite materials with excellent properties as needed [9–11]. For example, when polymer foam material is used as the core of sandwich composite [12–14], its impact resistance and energy absorption effect are significantly improved compared with similar materials [15,16]. With the development of the aviation industry, more and more aircraft structures have used polymer foam core sandwich composites. The craft, however, will encounter unexpected loads, such as bird strikes or other objects. In order to improve the impact resistance of aircraft, it is of great significance to study the energy absorption characteristics of polymer foam material.

Many scholars have conducted impact tests on materials, and the foam material exhibited obvious sensitivity to high strain rate [17–19]. Luong et al. carried out the Hopkinson pressure bar test on a very thin polyvinyl chloride (PVC) foam. However, because of factors such as the cellular structure and viscoelastic nature of the polymer, the evaluation of elevated strain rate properties of foams is challenging [20–22]. However, the standard test methods have some limitations in characterizing foams due to their large elastic strain, viscoelastic material characteristics, and high damage tolerance and the methods need to evolve for such materials [23–25].

The impact test of foam with intermediate strain rate loading was explored. The drop weight impact test has been widely used for characterizing the intermediate strain rate impact properties of foams [26,27], where a plate-like specimen is loaded under mid-point impact conditions [28]. This kind of testing allows for observing the extent of damage in the foam with respect to the distance from the impact location [14]. However, a limitation of this method is that the stress–strain diagram cannot be developed because only a small section of the specimen is subjected to direct loading. In the absence of complete fracture, there may be vibrations in the specimen and multiple impacts due to rebound (although air brakes and other methods can be used to minimize such effects). In addition, the results obtained from this kind PE impact cannot be compared to those obtained from compression tests due to the difference in the specimen loading configuration. The present work involved a modified drop weight impact instrumentation, where a standard hemispherical impact tup was replaced with a 25 mm diameter flat face tup to load a cylindrical specimen of the same diameter. The experiment allowed for developing the stress–strain diagram for the specimen and computing the energy absorption for comparison with those obtained from quasi-static and high strain rate loading conditions [29,30]. The experimental results of dynamic mechanical tests on foam materials showed that the density and temperature of the material will have a great influence on the mechanical properties and energy absorption effect of foam materials [31–34].

The impact test of foam with high strain rate loading was also explored. Experiments on the foams show that the strain in the foam is not uniform along the specimen length at high strain rates. The experimental results showed that the stress of the material increases with the increase in strain rate. The observation that the specimen deformation is nonuniform is also supported by finite element analysis simulations, which allowed for dividing the foam behavior into three modes based on strain rates: homogeneous mode, transitional mode, and dynamic mode. A split Hopkinson pressure bar is the most popular experimental method in the study of metal high strain loading. However, since the loading time and loading strain displacement of the split Hopkinson pressure bar have certain limitations, the condition of high strain rate loading for closed cell polymer foam of large thickness cannot be achieved. The results from impact tests are augmented with high strain rate loading results obtained from a shock tube-based test method [35–37]. Using a shock tube as a controlled experimental platform is very helpful for determining the high strain rate properties of materials. This test can provide the necessary data for material design. Shock tubes, having a single or a double diaphragm fracture mechanism to generate shock waves, have been widely used in aerodynamics research [38,39]. Shock tubes have also been used to study the effect of the shock wave on the deformation behavior of foams [40]. However, the previous shock tube-based studies were focused on the post-mortem of foams to observe the deformation and failure mechanisms. The shock tube developed in this work provides load–displacement data from the load cell, pressure transducers, and a high-speed camera and allows for comparing the energy absorption capability in other loading conditions. A transparent specimen chamber is constructed to allow for capturing the specimen deformation using a high-speed camera.

This work used a modified drop weight impact tower to conduct the testing of polyethylene (PE) foam at intermediate strain rate compression. The stress–strain curve of the foam at an intermediate strain rate was obtained. The results compared the energy absorption results with the values obtained under quasi-static compression tests. In order to study the energy absorption characteristics of polymer foam under high strain loading, a new method to obtain the energy absorption was found through theoretical derivation. An in-house developed shock tube test platform was used for the testing of PE foam at high strain rate compression. The energy absorption characteristics of PE foam under the impact were analyzed and are discussed.

2. Theory Analysis

2.1. Deformation Modes and Transitional Compression Velocity

The specimen deformation becomes progressively more localized as the compressive strain rate is increased and the deformation mode changes from homogeneous to transitional to shock mode, as shown in Figure 1 [41]. In the homogeneous mode, the stress values on the proximal and distal surfaces of the specimen are equal and the strain is distributed uniformly along the specimen length. However, when the compression velocity is large enough, the impacted foam will rapidly collapse and densify close to the proximal end. After sufficient densification, which depends on the strain rate, the stress is transferred to the next layer of cells in the specimen and this phenomenon continues either until the entire specimen is densified or until the strain is applied to the specimen. This effect becomes more pronounced as the compressive strain rate is increased. The stress transfer within the specimen from the proximal to distal end depends on the strain rate and total applied strain.
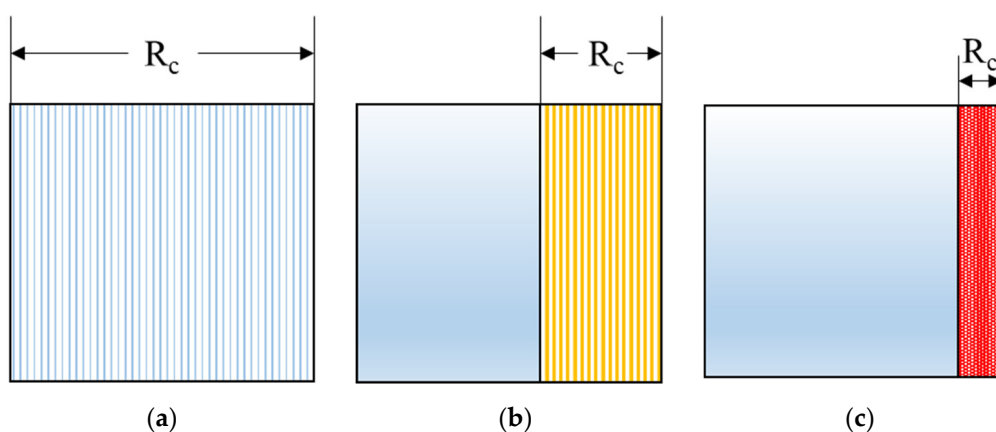

Figure 1. Three deformation modes of foam material under different loading rates [41]. R_c represents the compressed part. (**a**) Homogeneous mode: the stress values on the proximal and distal surfaces of the specimen are equal and the strain is distributed uniformly along the specimen length. (**b**) Transitional models: the impacted foam collapsed and the proximal end has not densified. (**c**) Shock mode: the impacted foam rapidly collapsed and densified close to the proximal end.

The rigid–linearly hardening plastic–locking (R-LHP-L) model is adopted to judge the three modes [42]. The first critical compression velocity that causes transition from homogeneous mode to transitional mode, V_{c1}, is described by [42]:

$$V_{c1} = \frac{\sigma_0}{9\rho_0\sqrt{\frac{E_1}{\rho_0}}} \tag{1}$$

where σ_0 is the yield stress of the material, ρ_0 is the density of the specimen in the original state, and E_1 is the strain hardening modulus of the material (Figure 2).

When the impact stress of σ_A inside the specimen is greater than the compaction stress of the specimen $\sigma_{(\varepsilon L)}$, the shock mode appears [41–44]:

$$\sigma_0 + \frac{\rho_0 V_s^2}{\varepsilon_L} \geq \sigma_0 + E_1\varepsilon_L \tag{2}$$

where V_s is the compression velocity of the foam, ε_L is the densification strain of the foam.

When the inequality above is equal, the second critical velocity is obtained, that is, the critical velocity for the shock mode to transitional mode:

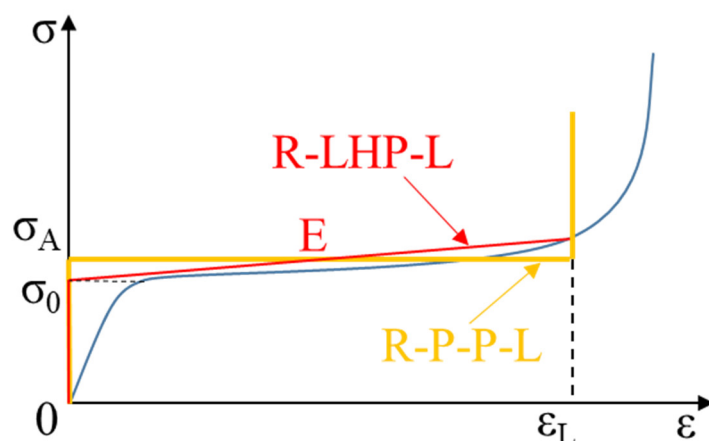$$V_{c2} = \varepsilon_L\sqrt{E_1/\rho_0} \tag{3}$$

Figure 2. Diagram of the stress σ of foam materials as a function of the strain ε, the green line is R-P-P-L model and the red line is R-LHP-L model [42]. Here, σ_0 is the yield stress of the material, ε_L is the locking strain of the material, E_1 is the hardening modulus of the material, and σ_{pl} is the plateau stress.

Therefore, when the deformation velocity of the specimen is less than V_{c1}, the specimen is in homogeneous mode. When the deformation velocity of the specimen is greater than V_{c1} and less than V_{c2}, the specimen is in the transitional mode. When the deformation velocity of the specimen is greater than V_{c2}, the specimen is in shock mode [41].

2.2. Energy Absorption

In homogeneous mode, the energy absorption of foam under plastic deformation can be calculated according to the stress–strain curve under quasi-static loading [45–47]:

$$Eq = D \int_0^{\varepsilon_L} \sigma(\varepsilon) d\varepsilon \tag{4}$$

where E_q is the energy absorption of foam under quasi-static loading, ε_L is the strain entering the densification phase, σ is the stress of the foam, D is the volume of the specimen.

In the transitional and shock modes, the strain in the foam is not uniform along the specimen length at high strain rates, which makes the calculation of the foam material unreliable. Therefore, we cannot get the strain–stress curve. Therefore, we have to find another way to calculate the energy absorption. According to [41], the impact energy can be divided into deformation energy and other energy loss, and can be given by:

$$E_i = E_s + E_w \tag{5}$$

where E_s and E_w are the energy absorption of foam under the high strain rate loading and the other energy loss, respectively.

According to the rigid–plastic–locking (R-P-P-L) model, the dynamic crushing stress σ_A at the proximal end is derived as [43,48–50]:

$$\sigma_A = \sigma_0 + \frac{\rho_0 V_s^2(t)}{\varepsilon_l} \tag{6}$$

The foam energy absorption is calculated by:

$$E_s = D \int_0^t \left(\sigma_A(t)\varepsilon_l + \frac{1}{2}\rho_0 V_s^2 \right) dt \tag{7}$$

The impact energy of the incident wave in the shock tube can be calculated by [51]:

$$E_i = \iint\limits_{0}^{t} p_s v_s ds dt \tag{8}$$

where E_i is the impact energy of the incident wave.

3. Experimental Testing

3.1. Specimen Details

Closed-cell polyethylene (PE) foam (Pregis, Aurora, IL, USA) with a density of 27.2 kg/m^3 was selected, as shown in Figure 3. The average diameter of the cells and the wall thickness were 1.49 mm and about 0.017 mm, respectively. Cylindrical specimens of 25.4 mm in diameter and height were used for testing. The Poisson's ratio of the material was found to range from 0.15 to 0.78.
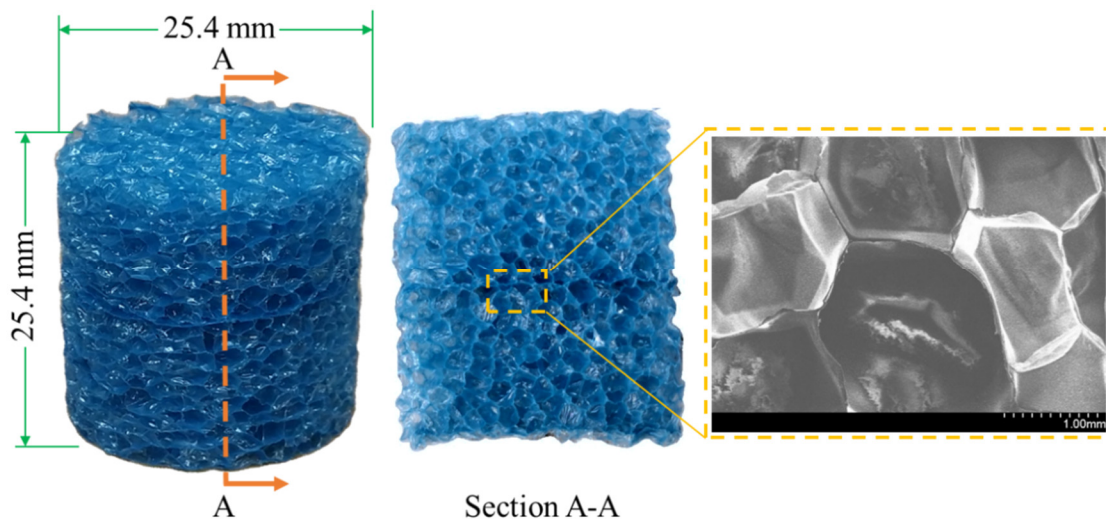

Figure 3. The structure of the PE foam specimen. The density is 27.2 kg/m^3, the average diameter and the wall thickness of the cell are 1.49 mm and about 0.017 mm, respectively. Both the diameter and height of the specimens are 25.4 mm.

3.2. Experimental Methods

The compression tests were conducted under three different loading conditions. The Instron 4467 (Instron, Norwood, MA, USA) universal test machine with a 30 kN load cell was used for quasi-static compression tests, as shown in Figure 4a. Nine specimens were tested under the quasi-static test (QSST), which were divided into three groups. The strain rates of these QSSTs were set at 10^{-3} s^{-1}, 10^{-2} s^{-1}, and 10^{-1} s^{-1}.

The intermediate strain rate compression tests were conducted on a modified Dynatup 9200 series drop weight impact tower, as shown in Figure 4b. The compressive force released during the impact between the impactor and specimen was measured by a dynamic load cell (PCB 208BC03, PCB, Depew, NY, USA), which was mounted under the specimen. The signal of the load cell was amplified and transmitted to an oscilloscope (Tektronix TDS 2014B, Tektronix, Inc., Beaverton, OR, USA) before being captured by a computer. A high-speed camera (NAC MEMRECAM HX-5, nac Americas, Ins., Salem, MA, USA) was used to capture the specimen deformation at a frame rate of 4000 Hz. An in-house Matlab code was developed to process the high-speed camera images to measure specimen deformation. The impact mass was 4 kg. The height of the impactor h was selected as 76 mm and 102 mm, and three specimens were tested for each one. The impact speed was 1.22 m/s and 1.4 m/s, respectively. The impact energies were 4 J and 3 J, respectively. The strain rates of these drop weight tests were set at 40 s^{-1} and 36 s^{-1}, respectively.
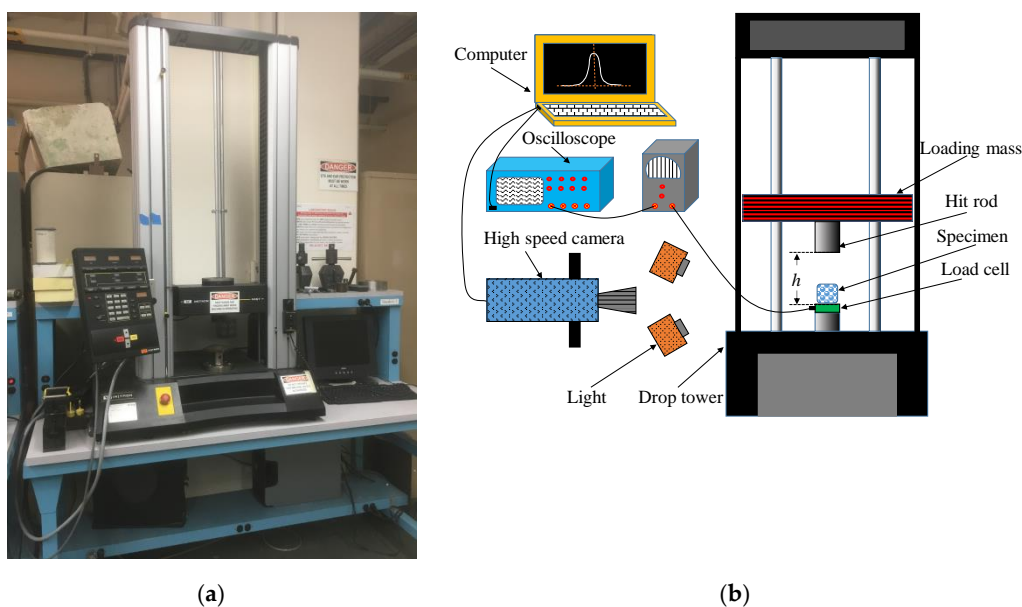
Figure 4. The experimental testing platform for foam materials: (**a**) the hydraulic testing machine corresponding to the quasi-static strain rate test; (**b**) the drop tower testing machine corresponding to the intermediate strain rate test.

The third group of tests were conducted at high strain rates using a double diaphragm aerodynamic shock tube. The stainless-steel shock tube had two driver chambers and one driven chamber, as shown in Figure 5. The diameters of the driver and driven chambers were 50.8 mm and 25.4 mm, respectively. An incident shock wave was generated after two diaphragms sequentially ruptured because of the difference in pressure set in the two driver chambers. This incident shock wave traveled through the driven chamber and interacted with the specimen placed in a transparent acrylic test chamber. L_d is the distance between two pressure sensors, and L_b is the distance between the second sensor and rigid plate. The pressure in the shock tube was measured by two pressure sensors (PCB 101A06, PCB, Depew, NY, USA) before being recorded by an oscilloscope (Tektronix TDS 2014B, Tektronix, Inc., Beaverton, OR, USA). Five specimens were tested, and their deformation was also captured by the high-speed camera with a frame rate at 100,000 Hz. The incident shock was set at 2.1 Mach.
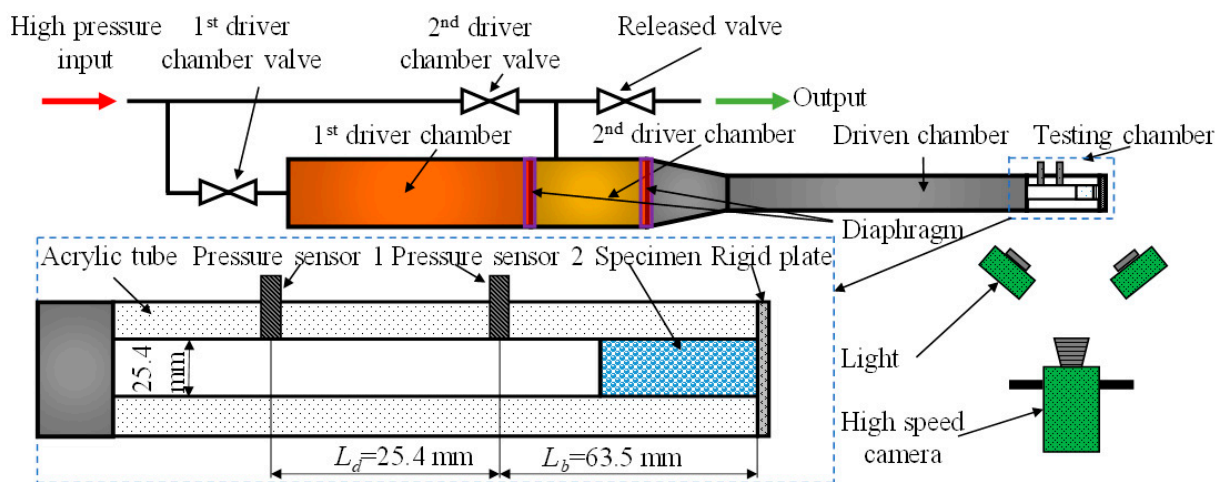

Figure 5. The shock tube experiment platform.

4. Results and Discussion

4.1. Stress–Strain Response

Representative force–time and stress–strain curves under QSST loading are shown in Figure 6. The curve shows a long stress plateau that corresponds to the high energy absorption under compression, then the stress rises sharply when entering the densification stage. The end of the stress plateau and onset of densification stage means the cell wall ruptured and the foam microstructure was permanently damaged. This is also a key factor in the foam's ability to absorb energy. The test was conducted at a strain rate of 10^{-3} s^{-1} calculated from Figure 6a, allowing uniform compression of the foam specimen, as the length L of the specimen and the strain rate of the compression specimen were known. Therefore, the force–time curve can be converted to obtain the stress–strain curve of the specimen, as shown in Figure 6b. According to reference [42], σ_0, ε_L, and E_1 can be obtained from the stress–strain curves.
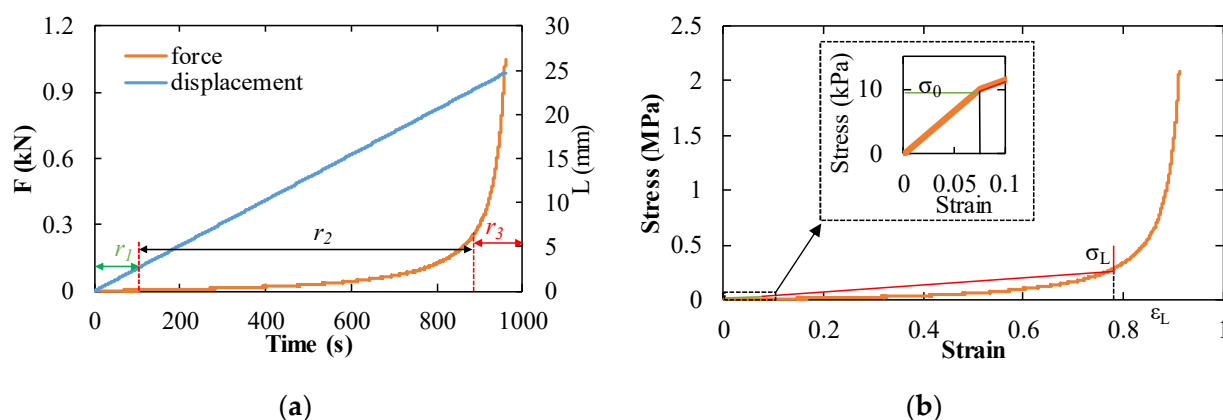

Figure 6. The mechanical response characteristics of foam materials in quasi-static experiments under a strain rate of 10^{-3} s^{-1}: (**a**) The diagram of the force and the displacement of foam materials as a function of the time, r_1 is the linear phase, r_2 is the plateau phase, and r_3 is the density phase, the orange line represents the force of the specimen, and the blue line represents the compression displacement of the specimen. Moreover, the whole deformation process of foam exhibited the linear phase, the plateau phase, and the density phase, respectively; (**b**) the diagram of the stress of the foam as a function of the strain, the yield stress σ_0 is 0.00998 MPa, the locking stress σ_L is 0.27 MPa, and the locking strain ε_L is 0.78.

In the drop weight experiment, the compressive force and the specimen length were simultaneously measured and are plotted over time in Figure 7a. In this figure, the specimen length steadily decreased at a constant rate while the compressive load increased moderately, and its rate turned to zero at the moment the compressive load reached the maximum value. This means that the specimen deformed at a constant strain rate in the elastic and plateau regions. Consequently, the stress–strain curve is shown in Figure 7b, and its strain rate was calculated over the proportional region of the specimen displacement–time relationship. The intermediate strain rate for this experiment was in the range of 40 s^{-1}.

The basic characteristics of the specimen deformation are similar to those at quasi-static loading. Here, a plateau region is followed by a densification stage. However, the plateau region shows significant vibration, as shown in Figure 7a. The deformation at an intermediate strain rate is not expected to be uniform along the specimen length. Hence, local microstructure variations in the foam affect the foam compression response observed in Figure 7b. According to the properties of foam, the plateau vibration represents the collapse activity of the stomatal unit. The magnitude of the vibration is determined by the number of stomatal units that collapse due to this initial cascade effect. In some foams, there is a wide range of stomatal sizes and stomatal wall thicknesses. Once a stomatal unit collapses, the stress is redistributed in the surrounding area and a new equilibrium is reached. The result is a smooth plateau with slow deformation. In the process of rapid

deformation, there is not enough time to redistribute the stress, which causes a significant vibration phenomenon.
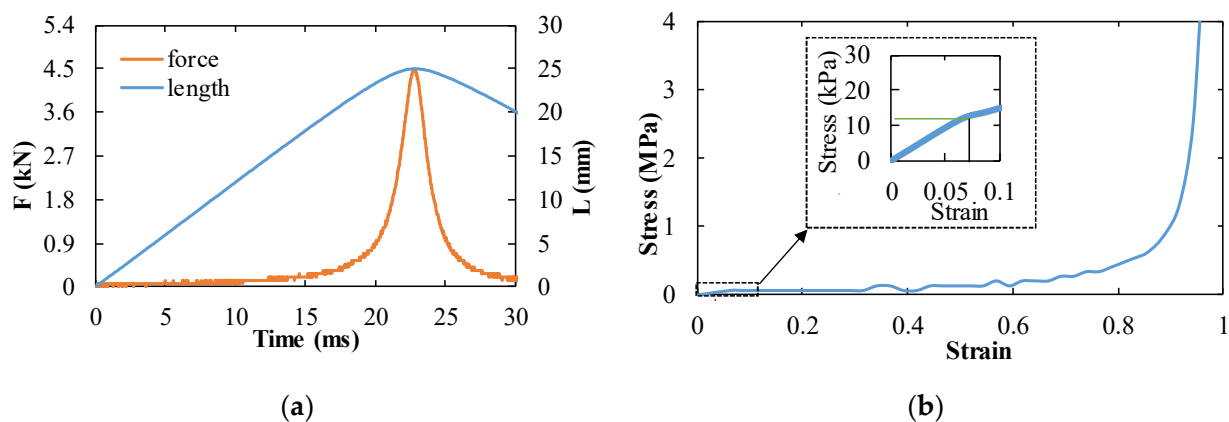

(a)

(b)

Figure 7. The mechanical response characteristics of the foam in intermediate experiments under a strain rate of 40 s^{-1}: (**a**) drop tower test curve corresponding to the displacement, force, and time of the experiment, the orange line represents the force of the specimen, and the blue line represents the compression displacement of the specimen; (**b**) the strain–stress curve of the foam in the drop tower experiments, here, the yield stress is 0.0109 MPa.

The representative shock test results of foam specimens are presented in Figure 8. The deformation velocity (V_s) of the specimen hovered around 155 m/s and the specimen deformation continued for 0.16 ms, as shown in Figure 8a. If the internal strain of the specimen is assumed to be uniform during the compression process, the strain rate of the specimen should be 6100 s^{-1}. However, in fact, the internal stress of the specimen was not uniform (this phenomenon will be shown in the next section), so it can be judged that the strain rate of the specimen was greater than 6100 s^{-1}, which is a high strain rate deformation. The pressure curve was obtained by the two pressure sensors mounted in the shock tube. The incident shock wave generated by the rupture of the diaphragm propagates in the driver chamber [38,39] and propagates under atmospheric pressure p_1. The pressure of the incident shock front is denoted as p_2 and recorded by two pressure sensors. When the incident wave hits the specimen, the first reflected wave p_s is generated. When the specimen is completely compressed and hits the rigid body, a second reflection wave (p_5) is generated. The pressures behind the shock wave, p_2, p_s, and p_5, all maintain a stable pressure value (see Figure 8b). During the shock wave compression of the specimen, the specimen was subjected to a constant pressure of p_s. The dynamic crushing stress σ_A can be calculated by Equation (6), where σ_0 can be obtained from the quasi-static tests and V_s can be obtained from Figure 8a. The stress–compression ratio curve of the specimen front during the whole compression is presented in Figure 8c. It can be argued that this figure does not present the stress–strain curve for the specimen, because that the specimen deformation behavior at such a high strain rate is not uniform and the strain is preferentially localized close to the specimen front surface.

4.2. Failure Mechanism

A representative set of specimens failed under quasi-static, intermediate, and high strain rate compression are shown in Figure 9a–c, respectively. Although the quasi-static (10^{-3} s^{-1}) and intermediate (40 s^{-1}) tests were conducted at four orders of magnitude of strain rate, the failure features of specimens are similar, which show that some plastic deformation is not recovered and densified cells scattered in the specimen. However, the shock tested (greater than 6100 s^{-1}) partially melts and resolidifies the specimen surface during the high strain rate deformation. The shock wave has a high temperature, which caused this phenomenon. The proximal part of the specimen (the top of the specimen in Figure 9c) shows densification due to the melting and a greater amount of damage than the

bottom part. When the specimen is opened, it can be seen that the changes in internal and external appearance are consistent. The cells inside were twisted, and many of the cells had a flat shape. Overall, the damage is nonuniform in the specimen along the length.
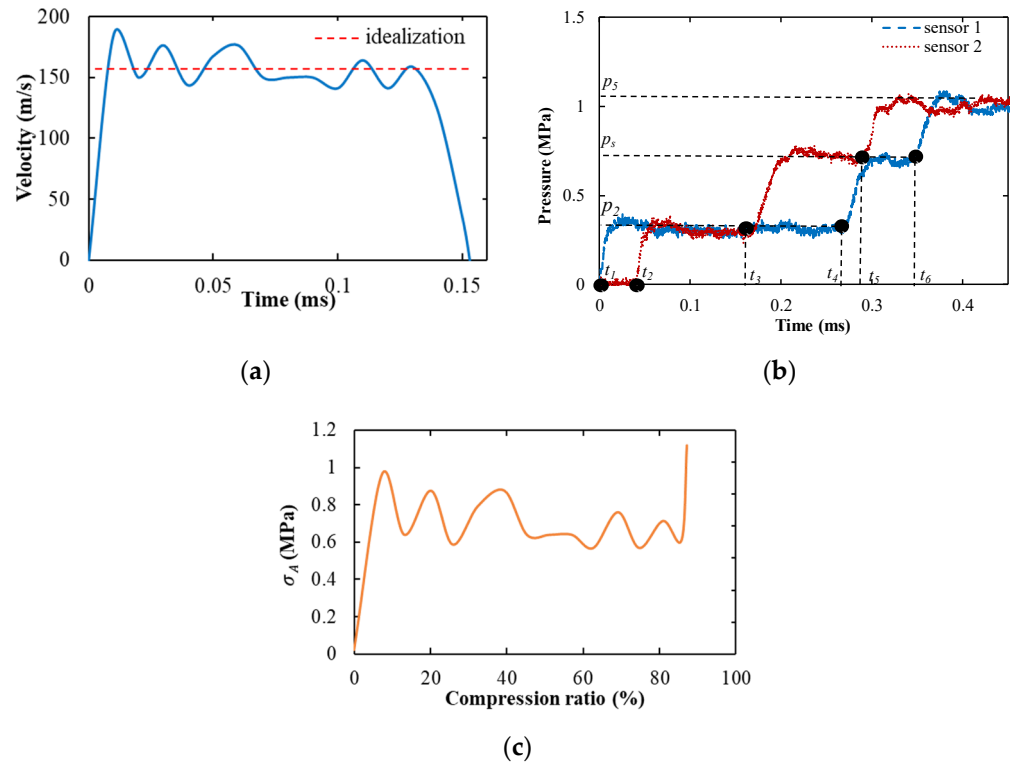

(**a**)

(**b**)

(**c**)

Figure 8. The testing results in the shock tube test: (**a**) the diagram of the velocity of the compression deformation as a function of the time, here, the blue line represents the experiment velocity and the red line represents the idealized velocity, and the average velocity of the compression is about 155 m/s; (**b**) the typical corresponding pressure–time curve of the shock tube, here, the blue line represents the pressure recorded by sensor 1 and the red line represents the pressure recorded by sensor 2, p_s represents the first reflected wave, and p_5 represents the second reflection wave; (**c**) the dynamic crushing stress σ_A as a function of the specimen compression ratio in the shock tube experiment, which was calculated by Equation (6).

These observations show that the specimen failure behavior transitions from uniform to nonuniform compression and the transition zone is greater than the strain rate of 40 s^{-1} tested in this work. The parameters σ_0, ε_L, and E_1 are obtained from the quasi-static curves of the specimen and are substituted into Equations (1) and (3), respectively, to obtain $V_{c1} = 1.3$ m/s and $V_{c2} = 26$ m/s. It is found that the tup velocity did not reach the condition of transition mode, while the velocity of shock wave reached the condition of shock mode.

The high-speed camera images, shown in Figure 10, also provide further evidence. The observations of drop weight impact in Figure 10a show that the center of the specimen has deformed preferentially, not the top part close to the impact. The deformation localization in the center is likely due to the area that triggered the initial failure of a few cells that led to preferential compression. Figure 10b includes the images of the specimen captured by the high-speed camera during shock testing. It can be seen from the picturesthat the overall deformation of the specimen is not uniform from the beginning of the test. The images at 0.04 and 0.08 ms show that the front part of the specimen was much more severely deformed than the back part. The images at 0.12 and 0.15 ms show a very interesting fact. The specimen front takes a concave shape, likely similar to the shape of the shock front at 0.12 ms and then it reverses to a convex shape at 0.15 when the shock reflects from the back part. This convex shape of the specimen is also visible in Figure 10b for the shock loaded

specimen, while the quasi-static and intermediate strain rate tested specimens show a flat front. Therefore, the experimental results agree with the theoretical expectation.
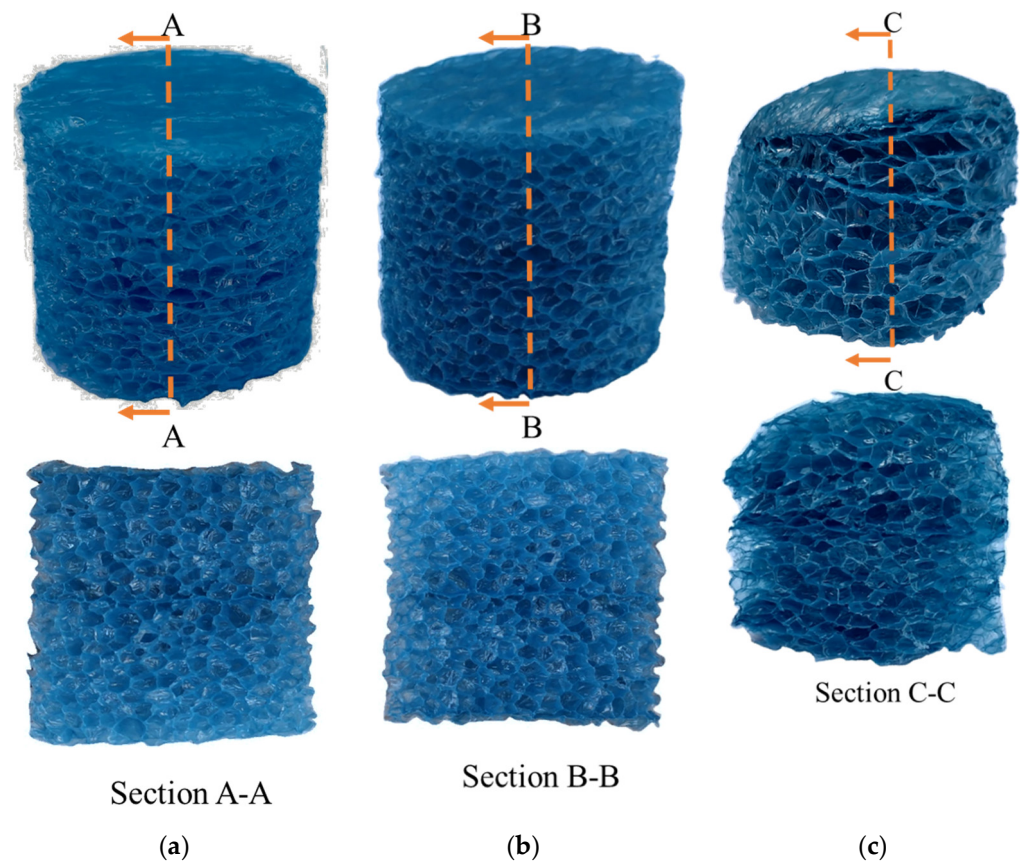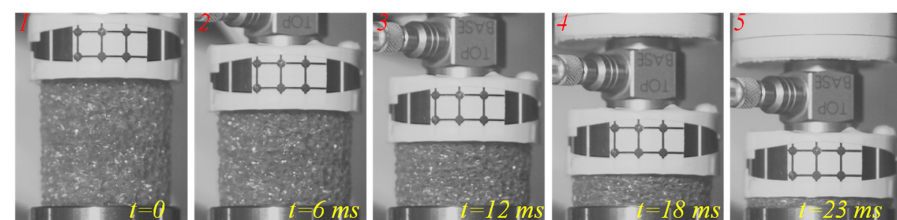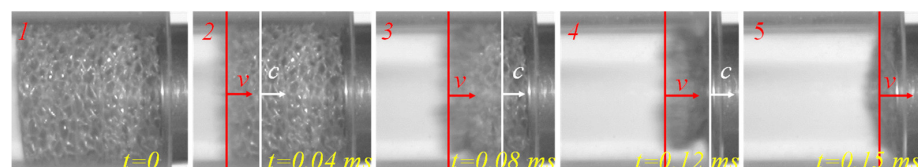

Figure 9. The final deformation of the foam under different loading rates, the bottom figures are the cross section of the specimens cut along the section marked in the top figures: (**a**) specimen failed under the quasi-static loading; (**b**) specimen failed under intermediate strain rate loading; (**c**) specimens failed under high strain rate loading.

Figure 10. The typical deformation progress of the foam in drop weight impact test and shock tube test: (**a**) drop weight impact test; (**b**) shock tube experiment. Here, v represents the velocity of the compression deformation, and c represents the impact velocity in the foam.

4.3. Energy Absorption

In order to further study the energy absorption state of the specimen under different strain rates, the deformation of the specimen under the quasi-static test and the drop weight test belong to the uniform mode deformation. Therefore, Equation (4) was used to calculate the energy absorption by the foam specimen tested under quasi-static and drop weight tests. The experimental deformation of the shock tube belongs to the shock mode deformation. Combining the specimen velocity curve with Equation (7), the energy absorption of the specimen can be calculated under the shock mode. The energy absorption characteristics of the foam under the three loading conditions are shown in Figure 11a. The energy density was calculated as a function of deformation strain for the quasi-static test and drop weight test, and the energy density was calculated as a function of the compression ratio for the shock mode test. The diagram shows a steady increase in the energy density in the elastic and plateau region. The energy density increases rapidly in the densification region after the compression ratio of the specimen reaches 0.7. The final total compression energy density of the specimen in quasi-static and intermediate strain rate reaches 0.1 MJ/m^3 and 0.17 MJ/m^3, respectively. It can be seen from the references that the energy density curves obtained are the same as those obtained in [52,53]. Moreover, the energy density trend under the shock loading condition was different. The specimen did not show any densification effect and the energy density was linear in the entire deformation range. The energy density at a high strain rate was higher than that for the quasi-static or intermediate strain rate range at any strain level. From the previous theoretical analysis, the specimen deformation is nonuniform under the shock loading condition, where the front face of the specimen compresses rapidly and enters the densification regime and then this deformation moves to the next layer of the foam upon further compression. Such an effect combines the elastic, plateau, and densification effects in a small zone and does not lead to the appearance of individual zones in the energy density curve for the entire specimen. The final energy density with the high strain rate is 0.34 MJ/m^3. Figure 11b shows the energy density for all the specimens. It can be seen that the energy density increases with the increase in the strain rate. The trends of energy density under high strain rate deformation in previous studies are similar to the results obtained in this test, as the energy density changed linearly with the increase in strain rate [54,55]. However, under a high strain rate, the energy density value varies in a wide range. This demonstrates that the energy density value is greatly affected by velocity under the shock mode.
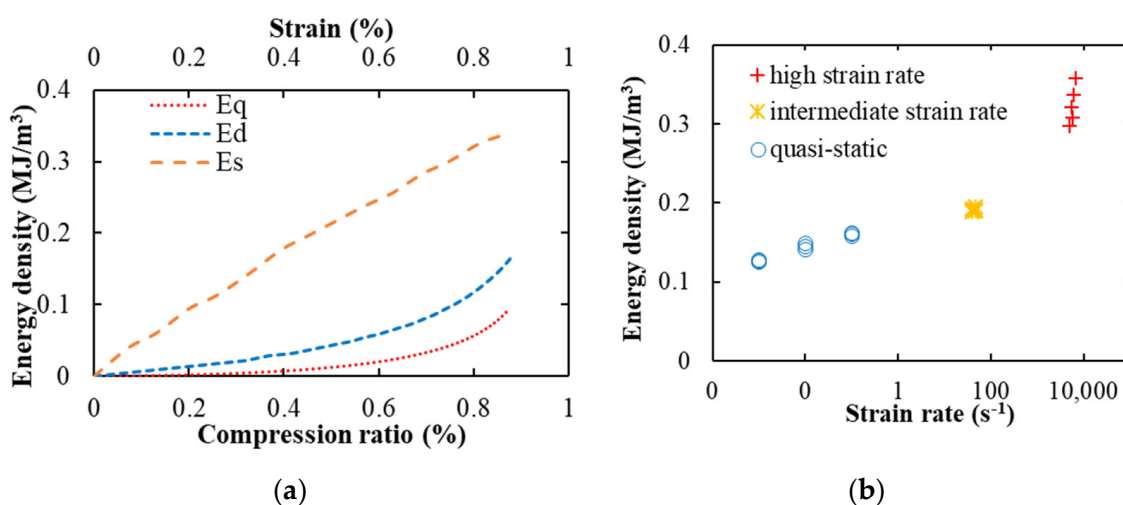

(a)　　　　　　　　　　(b)

Figure 11. The energy absorption of the foam under the different strain rates: (**a**) the diagram of the energy absorption as a function of the compression ratio, the red line (E$_q$) represents the energy absorption of the foam in the hydraulic test, the blue line (E$_d$) represents the energy absorption of the foam in the drop weight test, and the orange line (E$_s$) represents the energy absorption of foam in the shock tube test; (**b**) the energy absorptions of the foam under the different strain rates, here, the energy absorption value was greatly affected by velocity under the shock mode.

4.4. Discussion

The novel test method based on a shock tube has advantages of long loading time and high loading rates, which are useful in investigating the impact properties of foams at high strain rates. Here, the test theory is presented, and the test platform is designed with a special foam fixture and a visualization of the end of the tube, which is able to test foam impact properties and monitor the foam failure progress. Based on the test method, the failure progress and final failure modes of PE foams are discussed and, moreover, energy absorption capabilities of PE foams are assessed under both quasi-static and high strain rate loading conditions in this paper. However, as the core of sandwich composites, the energy absorption of foam is still unclear. In addition, research on foam core sandwich composites will also be carried out by combining the foam material with a skin in further work.

5. Conclusions

This work investigated the energy absorption capability of closed-cell polyethylene foams under both quasi-static and high strain rate loading conditions. Through theoretical derivation, the calculation method of the energy absorption of foam material under shock mode deformation is solved. It provides a new calculation method for obtaining the energy absorption value of foam material. A new method for obtaining the stress–strain curve of foams under intermediate strain rate deformation is provided by modifying a drop weight test machine. Here, both a modified drop weight impact method and the shock tube test method were used for foam shock testing at high strain rates. The deformation and the strain of the foam were studied by a high-speed camera and, moreover, the energy absorption of the foam under different loading rates is discussed. The following conclusions can be drawn from this study:

1. In this study, the first and second transitional velocities of PE foam compression mode are calculated. The results of the theoretical model agree with the experimental results, which verifies the theory.
2. The difference in PE foam material behavior in homogeneous mode and shock mode was observed through experiments. The specimen deformation varies as the strain rate changes. In the shock mode, the stress in the specimen is not uniform. Shock tests resulted in strain rates of $6.1 \times 10^3 \text{ s}^{-1}$, which were sufficiently high to cause selective densification in the proximal end of the specimen, as observed with a high-speed camera.
3. During the shock mode compression process, the energy absorption in the specimen varies linearly. When the speed is less than 1.3 m/s, this stable energy absorption state disappears. The energy density is greatly affected by velocity under the shock mode.

The above conclusion shows that the PE foam as a protective material for aircraft has good energy absorption characteristics. It can maximize its energy absorption characteristics and maintain stable energy absorption capacity under a high-speed impact.

Author Contributions: Writing—original draft, formal analysis, B.Y.; Writing—review & editing, validation, Y.Z. and Z.C. All authors have read and agreed to the published version of the manuscript.

Institutional Review Board Statement: Not applicable.

Informed Consent Statement: Not applicable.

Data Availability Statement: The data presented in this study are available on request from the corresponding author.

Conflicts of Interest: The authors declare no conflict of interest. The funders had no role in the design of the study; in the collection, analyses, or interpretation of data; in the writing of the manuscript, or in the decision to publish the results.

References

1. Youssef, G.; Reed, N.; Huynh, N.U.; Rosenow, B.; Manlulu, K. Experimentally-validated predictions of impact response of polyurea foams using viscoelasticity based on bulk properties. *Mech. Mater.* **2020**, *148*, 8. [CrossRef]
2. Hohe, J.; Beckmann, C.; Bohme, W.; Weise, J.; Reinfried, M.; Luthardt, F.; Rapp, F.; Diemert, J. An experimental and numerical survey into the potential of hybrid foams. *Mech. Mater.* **2019**, *136*, 15. [CrossRef]
3. Le Barbenchon, L.; Kopp, J.B.; Girardot, J.; Viot, P. Reinforcement of cellular materials with short fibres: Application to a bio-based cork multi-scale foam. *Mech. Mater.* **2020**, *142*, 13. [CrossRef]
4. Duan, Y.; Zhao, X.H.; Du, B.; Shi, X.P.; Zhao, H.; Hou, B.; Li, Y.L. Quasi-static compressive behavior and constitutive model of graded foams. *Int. J. Mech. Sci.* **2020**, *177*, 14. [CrossRef]
5. Drozdov, A.D.; Christiansen, J.D. Modeling the elastic response of polymer foams at finite deformations. *Int. J. Mech. Sci.* **2020**, *171*, 11. [CrossRef]
6. Cao, S.Z.; Liu, T.; Jones, A.; Tizani, W. Particle reinforced thermoplastic foams under quasi-static compression. *Mech. Mater.* **2019**, *136*, 17. [CrossRef]
7. Zhang, Y.; Jin, T.; Li, S.; Ruan, D.; Wang, Z.; Lu, G. Sample size effect on the mechanical behavior of aluminum foam. *Int. J. Mech. Sci.* **2019**, *151*, 622–638. [CrossRef]
8. Khosroshahi, S.F.; Olsson, R.; Wysocki, M.; Zaccariotto, M.; Galvanetto, U. Response of a helmet liner under biaxial loading. *Polym. Test.* **2018**, *72*, 110–114. [CrossRef]
9. Zhang, J.X.; Qin, Q.H.; Chen, S.J.; Yang, Y.; Ye, Y.; Xiang, C.P.; Wang, T.J. Low-velocity impact of multilayer sandwich beams with metal foam cores: Analytical, experimental, and numerical investigations. *J. Sandw. Struct. Mater.* **2020**, *22*, 626–657. [CrossRef]
10. Cetin, E.; Baykasoglu, C. Energy absorption of thin-walled tubes enhanced by lattice structures. *Int. J. Mech. Sci.* **2019**, *157*, 471–484. [CrossRef]
11. Munoz-Pascual, S.; Saiz-Arroyo, C.; Vuluga, Z.; Corobea, M.C.; Rodriguez-Perez, M.A. Foams with Enhanced Ductility and Impact Behavior Based on Polypropylene Composites. *Polymers* **2020**, *12*, 943. [CrossRef]
12. Kesavan, A.; Madhavan, V.R.B.; Chinnadurai, E. Mechanical and thermal properties of PVC and polyurethane foam hybrid composites. *Mater. Test.* **2020**, *62*, 544–552. [CrossRef]
13. Zhao, Z.; Jing, L. The response of clamped sandwich panels with layered-gradient aluminum foam cores to foam projectile impact. *Mech. Adv. Mater. Struct.* **2020**, *27*, 744–753. [CrossRef]
14. Ramirez, B.J.; Misra, U.; Gupta, V. Viscoelastic foam-filled lattice for high energy absorption. *Mech. Mater.* **2018**, *127*, 39–47. [CrossRef]
15. Zhu, Y.F.; Sun, Y.G. Dynamic response of foam core sandwich panel with composite facesheets during low-velocity impact and penetration. *Int. J. Impact Eng.* **2020**, *139*, 10. [CrossRef]
16. Pandey, A.; Muchhala, D.; Kumar, R.; Sriram, S.; Venkat, A.N.C.; Mondal, D.P. Flexural deformation behavior of carbon fiber reinforced aluminium hybrid foam sandwich structure. *Compos. Pt. B-Eng.* **2020**, *183*, 11. [CrossRef]
17. Borovinsek, M.; Vesenjak, M.; Hokamoto, K.; Ren, Z.R. An Experimental and Computational Study of the High-Velocity Impact of Low-Density Aluminum Foam. *Materials* **2020**, *13*, 1949. [CrossRef]
18. Guo, Y.; Yang, H.; Liu, X.; Zheng, Z.; Wang, J. Compressive mechanical behavior of closed cell Aluminum foam under dynamic loading. *J. Vib. Eng.* **2020**, *33*, 338–346.
19. Yang, B.; Cao, Z.; Chang, Z.; Zheng, G. The effect of the reflected shock wave on the foam material. *Int. J. Impact Eng.* **2021**, *149*, 103773. [CrossRef]
20. Xu, P.B.; Yu, Y.; Li, K.; Wu, X.T. SHPB experiment research on dynamic property of expanded polystyrene foam. *Polym. Test.* **2018**, *69*, 431–436. [CrossRef]
21. Johnsen, J.; Grytten, F.; Hopperstad, O.S.; Clausen, A.H. Influence of strain rate and temperature on the mechanical behaviour of rubber-modified polypropylene and cross-linked polyethylene. *Mech. Mater.* **2017**, *114*, 40–56. [CrossRef]
22. El-Qoubaa, Z.; Othman, R. Strain rate sensitivity of polyetheretherketone's compressive yield stress at low and high temperatures. *Mech. Mater.* **2016**, *95*, 15–27. [CrossRef]
23. Tang, N.H.; Lei, D.; Huang, D.W.; Xiao, R. Mechanical performance of polystyrene foam (EPS): Experimental and numerical analysis. *Polym. Test.* **2019**, *73*, 359–365. [CrossRef]
24. Henriques, I.R.; Rouleau, L.; Castello, D.A.; Borges, L.A.; Deu, J.F. Viscoelastic behavior of polymeric foams: Experiments and modeling. *Mech. Mater.* **2020**, *148*, 11. [CrossRef]
25. Bosi, F.; Pellegrino, S. Nonlinear thermomechanical response and constitutive modeling of viscoelastic polyethylene membranes. *Mech. Mater.* **2018**, *117*, 9–21. [CrossRef]
26. Li, Z.J.; Chen, W.S.; Hao, H. Mechanical properties of carbon foams under quasi-static and dynamic loading. *Int. J. Mech. Sci.* **2019**, *161*, 12. [CrossRef]
27. Ha, N.S.; Lu, G.X.; Xiang, X.M. High energy absorption efficiency of thin-walled conical corrugation tubes mimicking coconut tree configuration. *Int. J. Mech. Sci.* **2018**, *148*, 409–421. [CrossRef]

28. Ling, C.; Ivens, J.; Cardiff, P.; Gilchrist, M.D. Deformation response of EPS foam under combined compression-shear loading. Part II: High strain rate dynamic tests. *Int. J. Mech. Sci.* **2018**, *145*, 9–23. [CrossRef]

29. Zhang, H.; Zhou, Y.; Zhang, F.; Gong, W.; He, L. Studies on Foaming Properties and Mechanical Properties of Polypropylene /beta-Cyclodextrin Foamed Composite. *Mater. Rev.* **2020**, *34*, 04148.

30. Guo, Y.; Yang, H.; Liu, X.; He, S.; Wang, J. Dynamic mechanical properties of closed cell aluminum foam under medium and low strain rates. *J. Vib. Shock* **2020**, *39*, 282–288.

31. Das, S.; Rajak, D.K.; Khanna, S.; Mondal, D.P. Energy Absorption Behavior of Al-SiC-Graphene Composite Foam under a High Strain Rate. *Materials* **2020**, *13*, 783. [CrossRef] [PubMed]

32. Hwang, B.K.; Kim, S.K.; Kim, J.H.; Kim, J.D.; Lee, J.M. Dynamic compressive behavior of rigid polyurethane foam with various densities under different temperatures. *Int. J. Mech. Sci.* **2020**, *180*, 12. [CrossRef]

33. Guo, A.F.; Li, H.; Xu, J.; Li, J.F.; Li, F.Y. Effect of microstructure on the properties of polystyrene microporous foaming material. *e-Polymers* **2020**, *20*, 103–110. [CrossRef]

34. Krundaeva, A.; De Bruyne, G.; Gagliardi, F.; Van Paepegem, W. Dynamic compressive strength and crushing properties of expanded polystyrene foam for different strain rates and different temperatures. *Polym. Test.* **2016**, *55*, 61–68. [CrossRef]

35. Ouellet, S.; Frost, D.; Bouamoul, A. Using a shock tube to predict the response of polymeric foam to a blast loading. *J. Phys. IV Fr.* **2006**, *134*, 783–787. [CrossRef]

36. Levy, A. *Chapter 15.2—Shock Wave Propagation in Multi-Phase Media: 15.2 Weak Shock Wave Interaction with Inert Granular Media*; Elsevier Inc.: Amsterdam, The Netherlands, 2001.

37. Skews, B.W.; Levy, A.; Levi-Hevroni, D. Chapter 15.1—Shock Wave Propagation in Porous Media. In *Handbook on Shock Waves*; Elsevier Inc.: Amsterdam, The Netherlands, 2001.

38. Henshall, B.D. *The Use of Multiple Diaphragms in Shock Tubes*; Aeronautical Research Council: London, UK, 1955.

39. Alpher, R.A.; White, D.R. Flow in shock tubes with area change at the diaphragm section. *J. Fluid Mech.* **1958**, *3*, 457–470. [CrossRef]

40. Koohbor, B.; Ravindran, S.; Kidane, A. Effects of cell-wall instability and local failure on the response of closed-cell polymeric foams subjected to dynamic loading. *Mech. Mater.* **2018**, *116*, 67–76. [CrossRef]

41. Liu, Y.D.; Yu, J.L.; Zheng, Z.J.; Li, J.R. A numerical study on the rate sensitivity of cellular metals. *Int. J. Solids Struct.* **2009**, *46*, 3988–3998. [CrossRef]

42. Zheng, Z.; Liu, Y.; Yu, J.; Reid, S.R. Dynamic crushing of cellular materials: Continuum-based wave models for the transitional and shock modes. *Int. J. Impact Eng.* **2012**, *42*, 66–79. [CrossRef]

43. Zou, Z.; Reid, S.R.; Tan, P.J.; Li, S.; Harrigan, J.J. Dynamic crushing of honeycombs and features of shock fronts. *Int. J. Impact Eng.* **2009**, *36*, 165–176. [CrossRef]

44. Zheng, Z.J.; Yu, J.L.; Li, J.R. Dynamic crushing of 2D cellular structures: A finite element study. *Int. J. Impact Eng.* **2005**, *32*, 650–664. [CrossRef]

45. Avalle, M.; Belingardi, G.; Montanini, R. Characterization of polymeric structural foams under compressive impact loading by means of energy-absorption diagram. *Int. J. Impact Eng.* **2001**, *25*, 455–472. [CrossRef]

46. Rusch, K.C. Energy-absorbing characteristics of foamed polymers. *J. Appl. Polym. Sci.* **1970**, *14*, 1433–1447. [CrossRef]

47. Miltz, J.; Ramon, O. Energy absorption characteristics of polymeric foams used as cushioning materials. *Polym. Eng. Sci.* **1990**, *30*, 129–133. [CrossRef]

48. Tan, P.J.; Harrigan, J.J.; Reid, S.R. Inertia effects in uniaxial dynamic compression of a closed cell aluminium alloy foam. *Mater. Sci. Technol.* **2002**, *18*, 480–488. [CrossRef]

49. Tan, P.J.; Reid, S.R.; Harrigan, J.J.; Zou, Z.; Li, S. Dynamic compressive strength properties of aluminium foams. Part II—'shock' theory and comparison with experimental data and numerical models. *J. Mech. Phys. Solids* **2005**, *53*, 2206–2230. [CrossRef]

50. Reid, S.R.; Peng, C. Dynamic uniaxial crushing of wood. *Int. J. Impact Eng.* **1997**, *19*, 531–570. [CrossRef]

51. Jahnke, D.; Azadeh-Ranjbar, V.; Yildiz, S.; Andreopoulos, Y. Energy exchange in coupled interactions between a shock wave and metallic plates. *Int. J. Impact Eng.* **2017**, *106*, 86–102. [CrossRef]

52. Andena, L.; Caimmi, F.; Leonardi, L.; Nacucchi, M.; De Pascalis, F. Compression of polystyrene and polypropylene foams for energy absorption applications: A combined mechanical and microstructural study. *J. Cell. Plast.* **2019**, *55*, 49–72. [CrossRef]

53. Pei, L.; Guo, Y.B.; Zhou, M.W.; Shim, V.P.W. Response of anisotropic polyurethane foam to compression at different loading angles and strain rates. *Int. J. Impact Eng.* **2019**, *127*, 154–168.

54. Miralbes, R.; Ranz, D.; Ivens, J.; Gomez, J.A. Characterization of cork and cork agglomerates under compressive loads by means of energy absorption diagrams. *Eur. J. Wood Wood Prod.* **2020**, *79*, 719–731. [CrossRef]

55. Fan, Z.; Zhang, B.; Liu, Y.; Suo, T.; Xu, P.; Zhang, J. Interpenetrating phase composite foam based on porous aluminum skeleton for high energy absorption. *Polym. Test.* **2021**, *93*, 106917. [CrossRef]